Iran J. Earth Sci. 2026; 18(1): 81-96

Iranian Journal of Earth Science (IJES)

https://doi.org/10.57647/j.ijes.2025.16975

Original Research

Provenance and Depositional Environments of the Paleocene Kerman Formation in Central Iran

Seyyedeh Halimeh Hashemi Azizi[1,*], Payman Rezaee[2], Hosein Askari[2]

[1]*Department of Geology, Faculty of Sciences, Bu-Ali Sina University, Hamedan, Iran*
[2]*Department of Geology, Faculty of Sciences, University of Hormozgan, Bandar Abbas, Iran*

[*]**Corresponding author:** s.hashemiazizi@basu.ac.ir

Article History

Received:
31 August 2024

Revised:
19 October 2024

Accepted:
25 October 2024

Published online:
05 July 2025

Published in Issue:
31 March 2026

Abstract:

This paper discussed the depositional environment and provenance analysis of the siliciclastic rocks of the Kerman Formation for the first time. To determine the Kerman Formation's depositional environment and provenance sedimentological, petrographic, and geochemical investigations have been conducted accordingly. The Kerman Formation (~1017 m-thick), lithologically consisting of massive polymictic conglomerates interbedded with some minor sandstone layers, is well-exposed in NE Central Iran. Through detailed sedimentological studies, six lithofacies were recognized: matrix-supported massive conglomerate, matrix-supported conglomerate, clast-supported massive conglomerate, clast-supported crudely bedded conglomerate, horizontal bedded coarse to fine-grained sandstone, and massive coarse to fine-grained sandstone. The lithofacies associations of Gmm, Gmg, Gcm, and Sm are related to sedimentary gravity flow architectural elements and the lithofacies associations of Gh and Sh are related to channel-fill sandstone bodies architectural elements deposited in alluvial fan and braided fluvial systems. Petrographically, the Kerman Formation's conglomerate is categorized as a petromict conglomerate, and the sandstone is divided into volcanic arenite and feldspathic litharenite petrofacies. Gravels are made up mainly of basalt and andesite, as well as fewer limestone and agglomerated tuff. The sandstone plot on the QtFRF suggests that the sandstone of the Kerman Formation derived from volcanic lithic fragments. Geochemical analysis indicates a volcanic arc source area in an active margin tectonic setting, which can relate to the Sabzevar oceanic closure (a branch of Neotethys) volcanic activities. Low values of the Chemical Index of Alteration suggest cool and arid climate conditions alongside a near absence of intense alteration and recycled materials.

Keywords: Bardaskan; Fluvial architecture; Geochemistry; Paleogene; Terrestrial environment

Cite this article: Hashemi Azizi H., Rezaee P. & Askari H., (2026). "Provenance and Depositional Environments of the Paleocene Kerman Formation in Central Iran." *Iranian Journal of Earth Science*, *18*(1), 81-96. https://doi.org/10.57647/j.ijes.2025.16975

1. Introduction

The Central Iranian Microcontinent (CIM), which is itself a fragment of the larger Central Iran domain, represents an important and regionally extensive terrane in the eastern part of Iran (Berberian & King, 1981). Ophiolitic remnants of the Palaeo- and Neotethyan oceans surrounded the CIM. Sabzevar suture is a Neotethys-related structure, which is placed in the north of the Central Iranian Microcontinent between the Lut and Turan blocks (Rossetti et al., 2010; Shafaii Moghadam et al., 2014). This ophiolite occurrence represents the remnant of the Mesozoic oceanic or back-arc basin (GhasemShirazi et al., 2014; Omrani et al., 2013; Shafaii Moghadam et al., 2015). The Sabzevar oceanic domain existed during the Cretaceous (Rossetti et al., 2010; Shafaii Moghadam et al., 2014) and subducted below Eurasia during Paleocene times (Bröcker et al., 2021).

In NE Central Iran the Paleocene Kerman Formation crops out with a thrust lower boundary and eroded upper boundary with upper Cretaceous carbonate rocks and Eocene sandstone and marl, respectively. Previous work on the Kerman Formation revealed that this conglomerate sequence was formed due to orogenic movements at the beginning of the Paleogene period, which affected most of north and central Iran According to (Berberian & King, 1981), considerable parts of Cen-

tral Iran became land following the orogenic movements during the late Cretaceous. There was significant folding, magmatism, and uplift during the late Maastrichtian to Paleocene time in the rocks of Central Iran, which led to the emplacement of upper Paleocene - Eocene rocks on older rocks with a pronounced angular unconformity (Berberian & King, 1981).

(Huckriede et al., 1962) established the Kerman Formation type section, which is 300 meters thick and located seven kilometers north of Kerman. They reported that the conglomerate pebbles are composed of Cretaceous limestone in addition to Mesozoic and Paleozoic rocks; the lower contact with hippurites-bearing limestone appeared to be gradual. However, (Seyed-Emami, 1972) believed that the Kerman Formation lies with an angular unconformity on older rocks. The upper boundary in the type section is obscured, while toward the northeast the Kerman Formation is overlain by the Paleogene andesite and rhyolite volcanic rocks. The conglomerate beds which are distributed in Kerman, Tabas, and Lut Plain, covered by tertiary volcanic rocks are generally called the Kerman Formation which is equivalent to the Fajan Formation in Alborz, Pesteligh Formation in Kopet Dag, and probably the red shale of the Pabdeh Formation in Zagros. Central Iran's Paleocene conglomerate beds likely resulted from detrital sediments after the Laramide folding event; however, the upper Cretaceous strata gradually came into contact with the Paleocene conglomerate (Aghanabati, 2004). The researchers (Berberian & King, 1981; Huckriede et al., 1962; McCall, 1985; Seyed-Emami, 1972) hold different opinions regarding the age and location of this particular formation.

Lithofacies and petrofacies investigations are important to understanding the depositional processes (Abdel-Fattah & Sehsah, 2023; Bilal et al., 2023; Lee & Gihm, 2023; Smith & Platt, 2023; Zhang et al., 2021), besides, knowing the elemental composition through petrography and geochemical approaches creates an insight into the provenance and tectonic setting (Cui et al., 2024; Hashemi Azizi et al., 2018; Sangeeta et al., 2023). Mineralogical and geochemical analyses of siliciclastic rocks have been widely used to deduce provenance, tectonic setting, and palaeoweathering conditions of the source area, thus providing significant information helpful in palaeoenvironmental, palaeoclimatic, and palaeogeographical reconstructions (Akarish & El-Gohary, 2008; Bhatia, 1983; Bhatia & Crook, 1986; Dickinson et al., 1983; Jafari & Yazdi, 2014; Nesbitt et al., 1996; Sallam et al., 2022; Sallam & Ruban, 2021; Sallam & Wanas, 2019) Many analytical methods (petrological and geochemical) and discriminant functions with their plot diagrams were established by many workers for provenance specification (Bhatia, 1983; Bhatia & Crook, 1986; Dickinson et al., 1983; Roser & Korsch, 1988). Besides, some other function diagrams for tectonic setting discrimination of siliciclastic sediments were proposed by (Verma & Armstrong-Altrin, 2013; 2016). Deciphering the tectonic setting is the main way to understand provenance (Hashemi Azizi et al., 2018; Sallam & Ruban, 2021; Sallam & Wanas, 2019). Tectonic settings play the principal role in sedimentary environments, thus affecting the detrital sedimentary rock compositions. Footprints of the tectonic setting are particularly recognizable in first-cycle sediments, as they are not obscured by recycling and weathering. Therefore, the composition of the Kerman Formation's first-cycled sandstone and conglomerate are important for decoding the tectonic evolution of the region and depositional environment.

Despite previous studies on the stratigraphy, petrography, fossil content (allochthonous), and lower and upper boundary of the Kerman Formation (Berberian & King, 1981; Huckriede et al., 1962; McCall, 1985; Seyed-Emami, 1972), there is a lack of recent detailed information on lithofacies, petrofacies, and whole rock geochemistry of the Kerman formation in any areas of its outcrops. This research aims to fill this gap by examining the depositional conditions, provenance, and tectonic setting of the Kerman Formation by detailed sedimentological and geochemical investigations.

2. Geological setting

The Bardeskan area is located in NE Iran and is a part of the Central Iran sedimentary-structural unit. Figure 1 illustrates the location of the study area and other adjacent sedimentary-structural units in Iran. The region exhibits a range of rock units, extended from the Precambrian to the Quaternary. Metamorphic and igneous rocks are prevalent in this area. The Doruneh Fault is the largest and most active fault in the region which runs in an east-west direction. The Kerman Formation can be observed in multiple locations within the Bardeskan area. The Kerman Formation consists mainly of conglomerates, with occasional minor beds of red sandstone. The lithology of conglomerate clasts and sandstone has been attempted in a selected section of 1017 m. The conglomerate units are thick and massive, primarily composed of volcanic clasts. The Kerman Formation unconformably overlies the Upper Cretaceous carbonate rocks (Figure 2a); and is topped by Eocene sandstone and marls with erosional unconformity (Figure 2b).

The Kerman Formation in this area has rough and rugged exposure mostly of massive reddish and gray-colored conglomerates. The clast sizes in the conglomerates range from 2 to 210 mm, with the largest clast size at the base of the sequence being 210 mm, which gradually reduces to 76 mm towards the top of the sequence. The conglomerate layers are mostly clast-supported, with matrix-supported conglomerates being less common. In the lower 200 m of the sequence, the most conspicuous sedimentary structures are massive conglomerates, normal and inverse grading, and scoured lower contacts. The next 500 m of the sequence is dominated by horizontal bedding, while the upper 300 m exhibits a return to massive conglomerates, normal grading, and scoured lower contacts. Sandstone intercalations are primarily massive, coarse-grained, and red to

10.57647/j.ijes.2025.16975

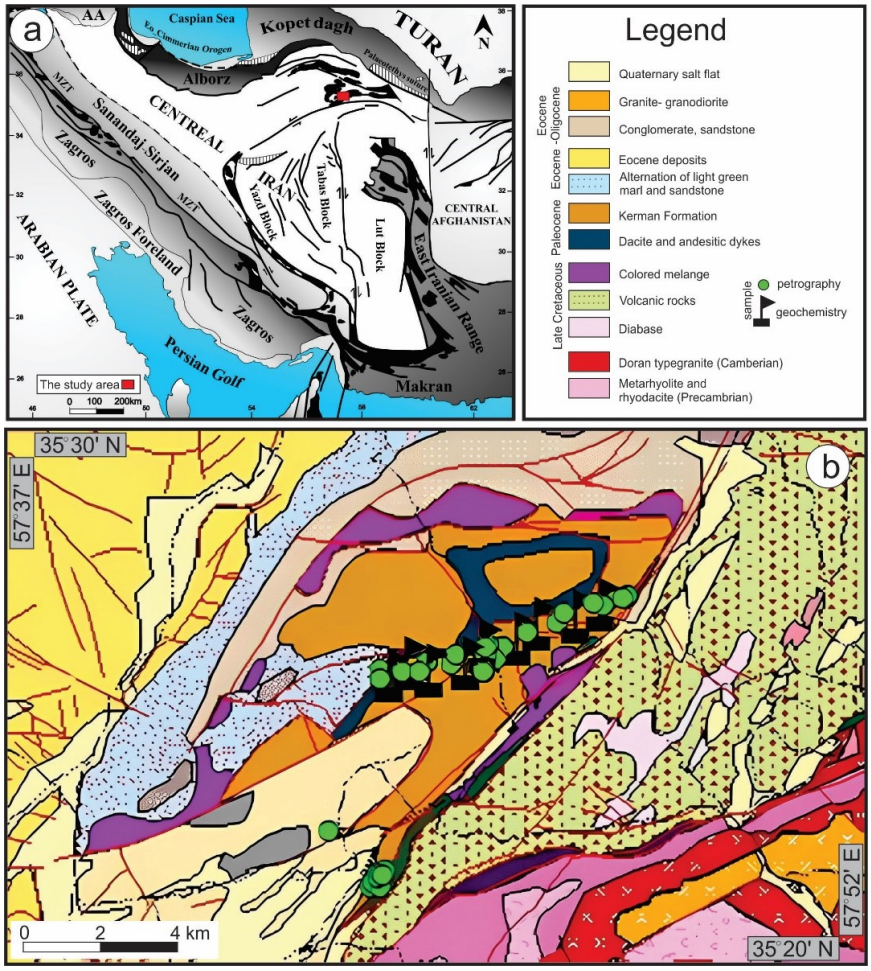

Figure 1. (a) Tectonic-structural map illustrating the sedimentary-structural units in Iran (Angiolini et al., 2007; Berberian & King, 1981); (b) Geologic map of the Bardeskan area (Shahrabi, 2010)

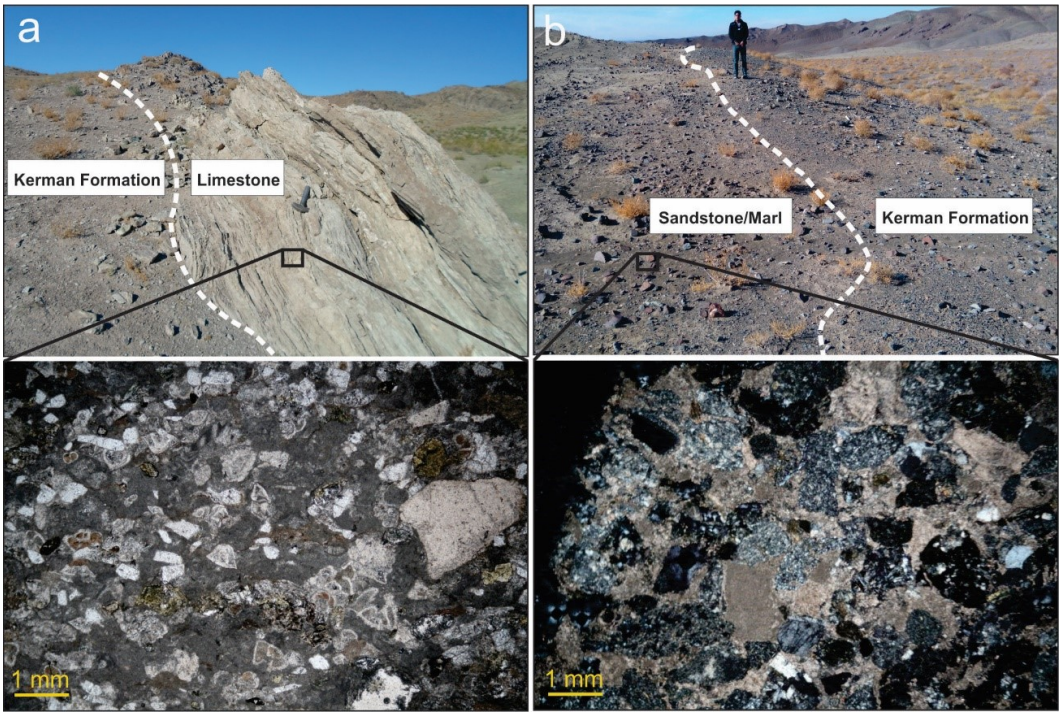

Figure 2. (a) Thrust lower boundary of the Kerman Formation; the inset picture is a fossiliferous limestone photomicrograph from the lower unit (PPL); (b) Erosional upper boundary of the Kerman Formation; the inset picture is a sandstone photomicrograph from the upper unit (XPL)

10.57647/j.ijes.2025.16975

gray, with some layers showing thin horizontal bedding, without a specific trend. The thickness of sandstone layers increases from 4-6 m to 16-21 m towards the top of the formation. The conglomerate parts have an overall thickness of 911.5 m, accounting for 89.6% of the formation, while the sandstone parts cover 10.4% of the formation with a total thickness of 105.5 m.

3. Materials and Methods

Sedimentary rocks were sampled from an outcrop of 1017 m-thick. Lithofacies investigation was conducted, including examining grain-size analysis, texture, degree of clast rounding and sorting, bed thickness, and sedimentary structures. After a detailed examination of 350 pebbles and 40 sandstone samples, 53 samples were selected for thin sections from which 25 are pebbles and 28 are sandstones. 10 selected sandstone samples underwent point-counting analysis based on the Gazzy-Dickinson method (Ingersoll et al., 1984). Lithofacies interpretation was carried out according to Miall's classifications (Miall, 1977; 1978; 2000), conglomerate petrofacies interpretation according to (Boggs, 2009), and sandstone petrofacies investigation using (Folk, 1980; Pettijohn et al., 1987) classifications.

Nine fresh fine-grained sandstone samples devoid of calcite veins were selected for whole-rock geochemical analysis. Major oxides (SiO_2, TiO_2, Al_2O_3, Fe_2O_3, MnO, MgO, CaO, Na_2O, K_2O, and P_2O_5) and trace element (V, Cr, Co, Ni, Y, Zr, Nb, Rb, Sr) concentrations were determined on a Philips PW 1480 *X*-ray spectrometer in AmethystLab in Iran. All Fe is reported as Fe_2O_3. The calculation of the Chemical Index of Alteration (CIA) was performed using molecular proportions, according to (Nesbitt & Young, 1982): CIA=100 $\times Al_2O_3$ / (Al_2O_3 + CaO* + Na_2O+K_2O), where CaO* represents the quantity of CaO included in the silicate fraction of the rock and quantified using a formula developed by Fedo et al. (1995): CaO* = mol CaO — mol CO_2(calcite) — (0.5 × mol CO_2)(dolomite) — [(10/3) × mol P_2O_5](apatite).

The index of compositional variability (ICV) is a helpful metric for evaluating the compositional maturity of fine-grained siliciclastics. To calculate the ICV, (Cox & Lowe, 1995) proposed the following formula: ICV = (Fe_2O_3 + K_2O + Na_2O + CaO + MgO + TiO_2)/Al_2O_3; in this equation, CaO includes the Ca sources related to detrital carbonate and phosphate. (Verma & Armstrong-Altrin, 2013) proposed a multi-element discrimination diagram used for tectonic discrimination. This diagram, partitioned into three main categories (arc, collision, and rift settings) is based on two discriminant functions using ten major oxides, including SiO_2, TiO_2, Al_2O_3, Fe_2O_3, MnO, MgO, CaO, Na_2O, K_2O, and P_2O_5.

4. Results

4.1 Analysis of the Kerman Formation Lithofacies

4.1.1 *Conglomerate (matrix-supported and clast-supported)*

The conglomerates of the Kerman Formation attain a thickness of 911.5 m and are composed of four lithofacies: matrix-supported massive conglomerate (Gmm), matrix-supported conglomerate (Gmg), clast-supported massive conglomerate (Gcm), clast-supported crudely bedded conglomerate (Gh). Sedimentary structures in these lithofacies include massive structures, inverse to normal grading, horizontal bedding, and erosive channels (Figure 3a-d). The grain size ranges from 2 to 210 mm; near the base, the average grain size is 65-180 mm, decreases to 53-95 mm in the middle and 25-75 mm at the top. Based on (Folk, 1980), roundness varies from angular to well-rounded, and sphericity is low to high. This diversity in size and shape of the grains may be attributed to proximal depositional conditions and heterogeneity in clast lithology (Hashemi Azizi et al., 2024).

- Matrix-supported massive conglomerate (Gmm)

An absence of layering and sedimentary structures characterizes this facies. The clasts are poorly sorted and are supported by a poorly sorted dark-colored matrix of sand, silt, and mud (Figure 4a). The clast sizes range from pebble to cobble, with some reaching up to 210 mm; their composition includes basalt, andesite, limestone, and siltstone. The clasts present a roundness spectrum from sub-rounded to well-rounded. Erosive lower bounding surfaces have appeared in some parts. The bed thickness can extend up to several meters. The textural and structural attributes of the Gmm suggest its deposition resulted from high-strength and viscous debris flow (Miall, 2006).

- Matrix-supported conglomerate (Gmg)

This facies is poorly sorted, normally and inverse graded (Figure 4b). It contains angular to sub-rounded gravels embedded in a poorly sorted matrix. The clast sizes range from 2 to 90 mm and the lithological composition is the same as facies Gmm. The lower bounding surface is prevalently abrasive, while the upper bounding contact is gradual. This facies thickness never exceeds 0.5 m. Deposition of the Gmg facies is attributed to low strength and viscous pseudoplastic debris flow (Miall, 2006).

- Clast-supported massive conglomerate (Gcm)

This facies is structureless, poorly sorted, and not graded. The clast sizes vary between pebbles and cobbles, reaching up to 170 mm. Mostly angular to sub-rounded in shape, these clasts display a color range from reddish to brown and gray (Figure 4c and d). This facies is mainly volcanic gravels, with minor limestone, siltstone, and agglomerate clasts. Certain areas exhibit the development of this lithofacies as channel fill. The formation of the Gcm facies can be attributed to high-energy pseudoplastic debris flow with its massive form resulting from high density and turbulent flow (Gagnon & Waldron, 2011; Kostic et al., 2005).

10.57647/j.ijes.2025.16975

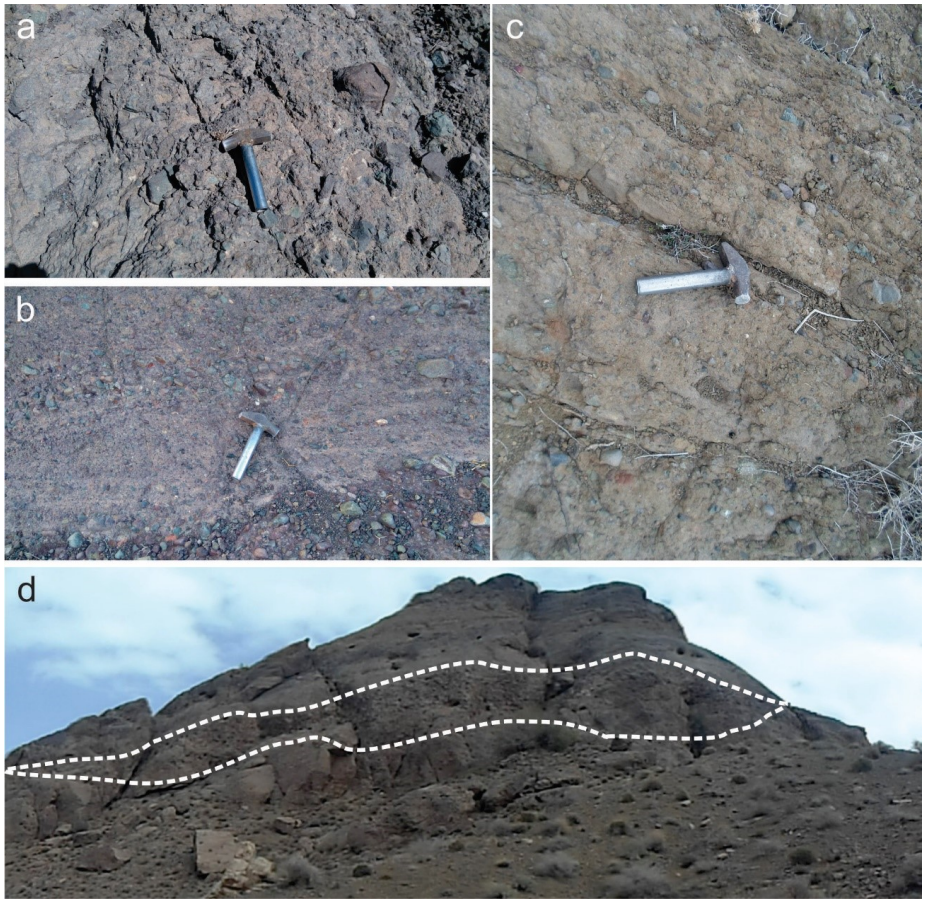

Figure 3. Selected outcrop views of sedimentary structures in conglomerate lithofacies; (a) Massive structure in clast-supported conglomerate; (b) Normal grading in matrix-supported conglomerate; (c) Horizontal bedding; (d) Channel

Figure 4. Selected outcrop views of conglomerate and sandstone lithofacies from the Kerman Formation; (a) Angular pebbles in poorly-sorted matrix in matrix-supported massive conglomerate (Gmm); (b) Normal grading in matrix-supported conglomerate (Gmg); (c) Angular pebbles in clast-supported massive conglomerate (Gcm); (d) Well-rounded pebbles in clast-supported massive conglomerate (Gcm); (e) and (f) Horizontal lamination in clast-supported, crudely bedded conglomerate (Gh); (g) Horizontal bedded, coarse to fine-grained sandstone (Sh); (h) Massive, coarse to fine-grained sandstone (Sm); (i) Faint lamination in massive, coarse to fine-grained sandstone

10.57647/j.ijes.2025.16975

- Clast-supported crudely bedded conglomerate (Gh)

The grain sizes vary from granule to pebble, with some cobbles. The horizontal stratification is crude and occasionally exhibits a quick upward fining trend, as illustrated in Figure 4e and f. The clast shapes are predominantly sub-rounded to well-rounded. The horizontally layered conglomerate in the research zone is mostly clast-supported with bed thicknesses generally reaching up to one meter. This lithofacies has been deposited through the migration of longitudinal bedforms, lag deposits on the channel floor, and sieve deposits (Miall, 2006). The Gh lithofacies features a clast-rich fabric deposited by high-energy, shallow tractional flow and high sediment concentration. Here, gravels are transported as bed load and sedimentation occurs during flow subsidence, occasionally as channel-fill. The horizontal stratification in this lithofacies is attributed to high sediment input, which leads to rapid lateral and downstream sediment accretion (Ghosh, 2014; Miall, 2006; Oplustil et al., 2005; Sridhar et al., 2013).

4.1.2 *Sandstones*

In the Kerman Formation, sandstones have a total thickness of 105.5 m, significantly less than conglomerates. The sandstone beds, primarily massive, exhibit hues of grey and red. While they are chiefly devoid of distinct stratification, occasional limited lamination, and horizontal bedding can be spotted (Figure 4g-i). The grain size within these sandstones varies from medium to very coarse, with a general trend of decreasing upward. The microscopic investigation shows these sandstones have poor to medium sorting (Hashemi Azizi et al., 2024).

- Horizontal bedded coarse to fine-grained sandstone (Sh)

The Sh facies contains coarse-grained pebbly sandstones, with poor sorting and horizontal bedding (Figure 4g). The horizontally bedded sandstone is deposited by plane-bed flow (critical flow) according to (Miall, 2006).

- Massive, coarse to fine-grained sandstone (Sm)

This facies is structureless and the grains are fine to coarse with poor sorting, combined with pebble-sized grains, sometimes displaying faint lamination (Figure 4h and i). Angular grains accompanied by poor sorting in Sm lithofacies indicate deposition from sediment gravity flows of (Miall, 2006).

Table 1 summarizes the lithofacies of the Kerman Formation.

4.2 Analysis of the Kerman Formation Petrofacies

Figure 5 illustrates the clast lithology and the distribution of each lithology type within the Kerman Formation conglomerate. Predominantly, basalt forms the major composition of gravels, followed by andesite, limestone, and agglomerated tuff in descending order of abundance. Selected photomicrographs of gravels are shown in Figure 6. Polymictic microconglomerates also contain unstable volcanic clasts and fewer limestone fragments (Figure 7a–d), thus can be classified as a petromict conglomerate according to (Boggs, 2009). Regarding the significant percentage of basalt and andesite rock fragments, it is classified as an intermediate and mafic volcanic conglomerate, in terms of chemical composition (Boggs, 2009). Pebble sizes reach 15 mm under the microscope and are rounded to well-rounded with poorly to medium sorting.

To identify the petrographic composition and sandstone type, 10 sandstones were selected for point-counting analysis; the obtained data are in Table 2. The data were plotted in the ternary diagram from (Folk, 1980). and mainly dropped into two areas of volcanic arenite and feldspathic litharenite (Figure 8). Volcanic arenite petrofacies contains 35–55% of rock fragments mostly volcanic and occasionally sedimentary (fossiliferous limestone). Feldspars reach 15% and potassium feldspars are more than plagioclases. Fine-grained textures are 15% and quartz content hardly reaches 5%. The maturity varies from immature to sub-mature (Figure 7e–f). Feldspathic litharenite comprises 45% rock fragments mainly mafic to intermediate volcaniclastics and rarely sedimentary. Felspars and quartz content are 35 and 10% respectively. Fine-grained textures reach 20%. The maturity of feldspathic litharenite is similar to the volcanic arenite (Figure 7g–h). Most of the sandstone samples from the Kerman Formation contain volcanic detritus represented by lithic fragments and single phenocrysts (Figure 7). Quartz grains show straight extinction. Volcanic clasts from the Kerman Formation show microlithic, lathwork, and vitric homogeneous textures (Figure 7).

4.3 Whole-rock geochemistry

Sandstones from the Kerman Formation display low major element concentrations compared with average upper and middle continental crust composition, Fe_2O_3 is exceptional with high concentration (Rudnick & Gao, 2003); the SiO_2 average content is 43.09–65.93 wt.%, the Al_2O_3 is 8.82–13.75 wt.%, the TiO_2 average content is 0.3–0.57 wt.%, the Fe_2O_3 average content is 3.5–8.38 wt.%, and CaO has a variable total content of 3.79–9.22 wt.% and two samples with 15.82 and 20.48 wt.% (see Table 3). The carbonate content can be affected by secondary activities like calcium carbonate cementation as observed in thin sections. CaO and LOI show a positive linear correlation for all sandstone samples from the Kerman Formation. The samples have high trace element concentrations (Appendix) in Cr (129–1116 ppm), Ni (86–395ppm), Sr (319–689 ppm), V (48–120 ppm), and Zr (94–188 ppm), and low concentrations in Ba (109–332 ppm) compared with upper continental crust (UCC) composition (Rudnick & Gao, 2003). The CIA mean values of the analyzed sandstone samples are 34.21. The ICV values of these samples range from 1.4 to 3.7 indicating fresh andesite to fresh basalt (see Ap-

Table 1. Summary of lithofacies in the Kerman Formation

Lithofacies and code	Lithology	Sedimentary structures	Interpretation
Gmm: matrix-supported massive conglomerate	Grey to brown polymictic orthoconglomerate; angular to sub-rounded volcanic and sedimentary cobble- to pebble-sized clasts embedded in a poorly sorted matrix of sand, silt, and mud.	Massive structureless beds; occasional normal grading; occurrences of crude horizontal stratification; scoured lower surfaces; several meters of bed thickness.	High-strength and viscous debris flow
Gmg: matrix-supported conglomerate	Red to brown polymictic orthoconglomerate; matrix-supported sub-rounded to rounded volcanic and sedimentary pebble- to granule-sized conglomerate; poorly sorted	Normal and inverse grading; scoured lower surfaces	Low-strength and viscous pseudoplastic debris flow
Gcm: clast-supported massive conglomerate	Grey to brown polymictic conglomerate; poorly sorted, angular to rounded cobble- to pebble-sized clasts	Massive, structureless beds; intercalation with matrix-supported conglomerate with normal and inverse grading; occurrences of crude horizontal stratification; channel fill	High-energy pseudoplastic debris flow; massive form resulting from high density and turbulent flow
Gh: Clast-supported, crudely bedded conglomerate	Brown to red polymictic conglomerate; sub-rounded to well-rounded pebble- to granule-sized clasts in poorly sorted matrix	Crude horizontal stratification; occasional quick upward fining trend; intercalation with clast-supported massive conglomerate	Bed load sheets; channel-fill; high sediment input which subsequently leads to rapid lateral and downstream sediment accretion
Sh: Horizontal bedded, coarse to fine-grained sandstone	Gray to red coarse-grained to pebbly sandstones; poorly sorted	Horizontal stratification; interbedding with matrix- and clast-supported conglomerate beds	Plane-bed flow (critical flow)
Sm: Massive, coarse to fine-grained sandstone	Gray to red coarse-grained to pebbly sandstones; poorly sorted	Massive structureless layers; Crude thin lamination; interbedding with matrix- and clast-supported conglomerate beds	sediment gravity flows

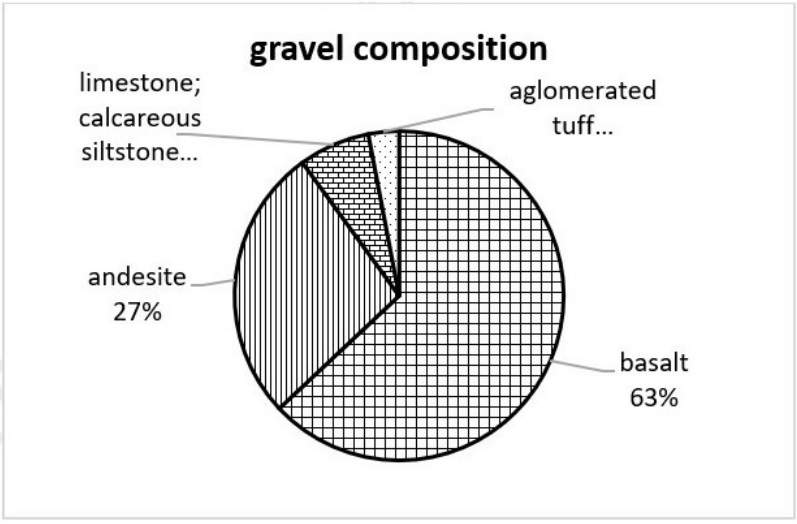

Figure 5. The petrography and percentage of the diagnosed gravels in the conglomerate of the Kerman Formation

10.57647/j.ijes.2025.16975

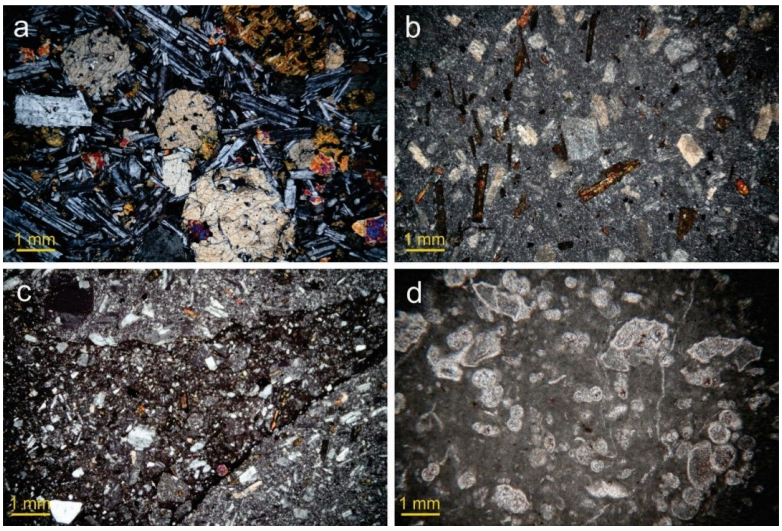

Figure 6. Selected photomicrographs of gravels from the Kerman Formation; (a) Basalt contains imbricated plagioclases and clinopyroxene grains (XPL); (b) Andesite contains elongated brownish amphibole, sanidine, and vitric groundmass (XPL); (c) Agglomerate tuff (XPL); (d) Globotruncana-bearing limestone (PPL)

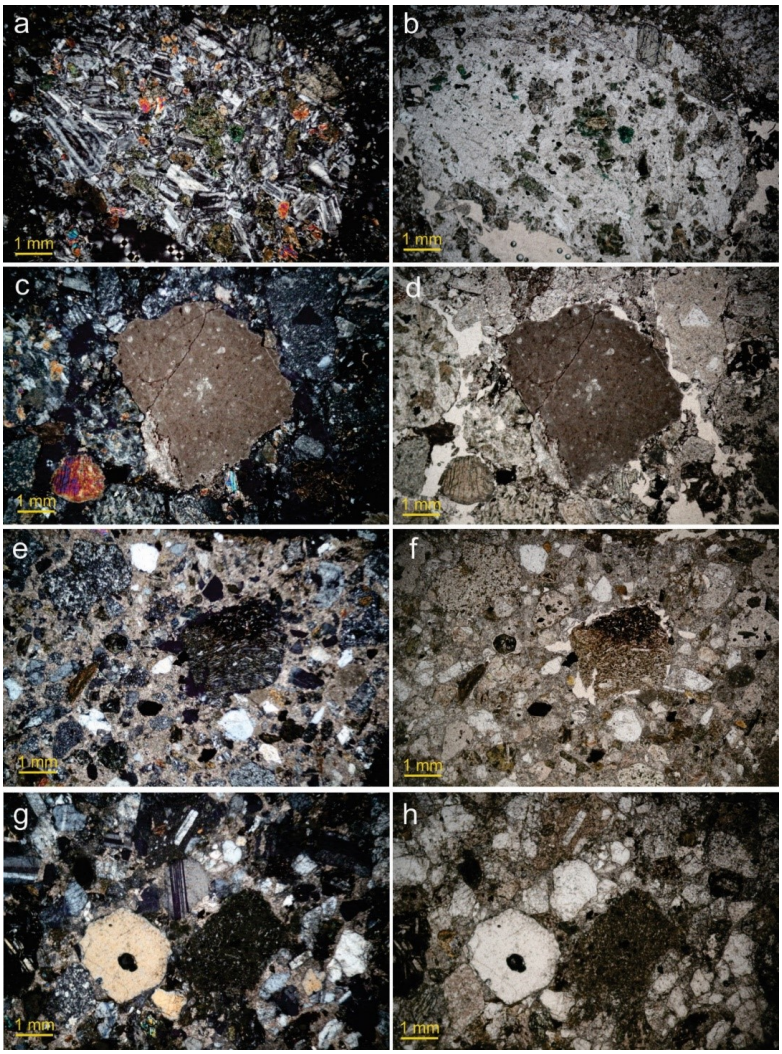

Figure 7. Selected photomicrographs of conglomerate and sandstone petrofacies from the Kerman Formation; (a) Petromict conglomerate, a basalt pebble is obvious in the middle of the photo (XPL) and (b) (PPL); (c) Petromict conglomerate, a limestone pebble is conspicuous in the middle of the photo (XPL) and (d) (PPL); (e) Volcanic arenite sandstone, volcaniclastic lithic fragments are spread across the sample in a carbonate cement (probably secondary) (XPL) and (f) (PPL); (g) Feldspathic litharenite sandstone, plagioclase and quartz grains are adjacent to the volcaniclastic lithic fragments (XPL) and (h) (PPL)

10.57647/j.ijes.2025.16975

Table 2. Point-counting data from 10 sandstone thin sections of the Kerman Formation. Qm: monocrystalline quartz; Qp: polycrystalline quartz; Qt: Qm+Qp; P: plagioclase; K: potassium feldspar; F: P+K; Ls: sedimentary lithic fragments; Lv: volcanic lithic fragments; Lm: metamorphic lithic fragments; Lt: Ls+Lv+Lm

sample#	Qm	Qp	Qt	P	K	F	Ls	Lv	Lm	Lt	total	Qt%	F%	Lt%	Ls%	Lv%	Lm%
KS1	75	2	77	89	179	268	159	331	26	516	861	8.9	31.1	59.9	30.9	64.1	5
KS2	37	0	37	73	197	270	137	295	9	441	748	4.9	36	58.9	31	66.9	2
KS3	37	2	39	21	56	77	115	378	34	527	643	6	11.9	81.9	21.9	71.7	6.4
KS4	42	0	42	5	33	38	86	367	3	456	536	7.8	7	85	18.9	80.4	0.6
KS5	36	0	36	12	18	30	67	454	11	532	598	6	5	88.9	12.6	85.3	2
KS6	30	0	30	34	94	128	53	529	14	596	754	3.9	16.9	79	8.9	88.7	2.3
KS7	45	1	46	48	144	192	97	549	29	675	913	5	21	73.9	14.3	81.3	4.3
KS8	69	0	69	11	161	172	78	293	23	394	635	10.8	27	62	19.8	74.3	5.8
KS9	23	0	23	19	79	98	37	401	14	452	573	4	17.1	78.8	8.2	88.7	3
KS10	88	1	89	154	204	358	124	312	17	453	900	9.8	39.7	50.3	27.4	68.9	3.7

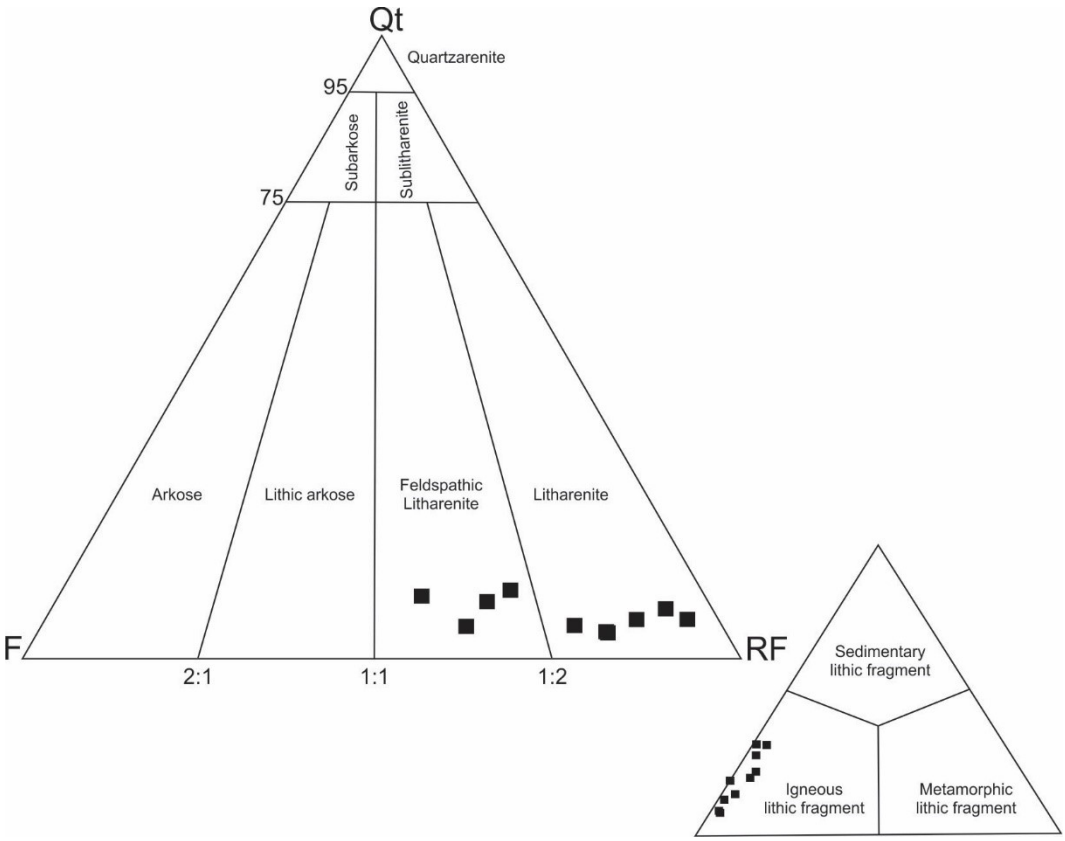

Figure 8. Data from point-counting analysis plotted on the Folk (1980) sandstone petrofacies ternary diagram

10.57647/j.ijes.2025.16975

pendix).

5. Discussion

5.1 Depositional environment

The typical sedimentary characteristics of the Kerman Formation are commonly very coarse- to coarse-grained composition, massive geometry, horizontal lamination, disorganized bed, inverse and normal grading, and faint lamination. The sedimentary log shows the full profile of a fluvial environment (Figure 9). Clast- and matrix-supported thick-bedded conglomerate intercalated with 3–6 m sandstone, with a mild fining upward, can be seen throughout the studied section. Matrix-supported massive conglomerate (Gmm), matrix-supported conglomerate (Gmg), clast-supported massive conglomerate (Gcm), and massive, coarse to fine-grained sandstone (Sm) lithofacies association are related to sedimentary gravity flow (SG) architectural elements (Hashemi Azizi et al., 2024). The SG architectural element is commonly established in alluvial fans and proximal braided river systems through sediment-gravity debris flow with a high sedimentation rate (Ghoshal et al., 2010; Miall, 2000; 2006). Clast-supported, crudely bedded conglomerate (Gh) and horizontal bedded, coarse to fine-grained sandstone (Sh) lithofacies association are related to channel-fill sandstone bodies (CH) architectural elements (Miall, 2006).

Field observations such as normal grading sequences (finning upward), absence of floodplain fine-grained depositions, and high thickness of conglomerate beds, along with distinguished lithofacies and their lateral changes provide valuable insights into the Kerman Formation's depositional environment. Comparison with Miall fluvial models (Miall, 1985; 2006; Nichols, 2009) suggest that the Kerman Formation was deposited in both alluvial fan and proximal braided fluvial systems, indicating a close connection between these environments. (Zhang et al., 2020) reviewed the alluvial fans and concluded the following characteristics. Gravity flow and sheet flow are alluvial fans' main sediment transport mechanisms. Sediments of alluvial fans are characterized by debris flow chaotic accumulation, and low textural maturity and ordering degree. Alluvial fans also have low sub-facies stability in their internal structures. Considering the steep slope of alluvial fans, their proximity to the provenance, and their small area, sediments of debris flow, channel, and sheet flood reflect changes of the provenance extensively and have frequent changes in facies. The studied section of the Kerman Formation involved all the above characteristics confirming the depositional situation of the alluvial fan system.

5.2 Provenance and tectonic setting

Sandstones from the Kerman Formation contain first-cycled volcanic inputs, including lithic fragments and single phenocrysts of quartz and feldspars. These volcanic lithic fragments show microlithic, vitric homogeneous, and lathwork textures. In an active arc setting different types of volcanic activity show different textures in volcano-clastic rocks, thus pure volcanolithic sandstones testify direct relations with the types of volcanic activity within the arc (Critelli et al., 2002; Marsaglia et al., 2016). As noted by (Critelli & Ingersoll, 1995), the fragmentation of intrabasinal basaltic and andesitic lava flows tends to create volcanolithic sandstone, which includes an abundance of vitric, microlithic, and lathwork volcanic lithics; the gravels of the Kerman Formation with basaltic and andesitic compositions confirm this.

Relatively low SiO_2 and high Fe_2O_3, Cr, and V content in the Kerman Formation samples indicate mainly mafic magmatic arc input (McLennan et al., 1993; Nesbitt & Young, 1982). As mentioned earlier, the total CaO and LOI index has a positive linear correlation that conveys the presence of carbonate-bearing minerals such as calcite in analyzed sandstone samples from the Kerman Formation. Chemical weathering alters intensively the major element geochemistry and mineralogy of siliciclastic sediments (McLennan et al., 1993; Nesbitt & Young, 1982).

The chemical index of alteration (CIA; (Nesbitt & Young, 1982)) is a functional way to evaluate the degree of chemical weathering. High values of the CIA index, over 90%, convey considerable conversion of feldspar to clay and therefore intense weathering. Low values of the CIA in Kerman siliciclastic rocks (Table 3) show the near absence of intense alteration and even recycled materials, it also might be evidence of cool or arid climate conditions according to (Fedo et al., 1995). The index of compositional variability (ICV) is another approach to assessing the number of weathered minerals in siliciclastic rocks. The ICV values for the analyzed samples of the Kerman Formation (Table 3) imply unweathered fresh detrital minerals took place in first-cycle deposits according to (Cox & Lowe, 1995). The plot of CIA against ICV (Potter et al., 2005) indicates fresh andesite to fresh basalt as a source rock for the Kerman sandstone samples (Figure 10a).

CIA has a linear trend for the sandstone samples of the Kerman Formation ranging from 17.7 to 45.6. A–CN–K trend and CIA ratios, based on (Roser et al., 2002), can be affected by tectonism in both active tectonic settings and stable margins. In the case of Kerman Formation samples, the linear trend of sandstones from fresh basalt to fresh andesite implies the uplift and emplacement of fresh volcanic rocks in active tectonic settings (Figure 10b).

Chemical compositions of clastic sedimentary rocks may point out the tectonic setting of the source areas (Armstrong-Altrin et al., 2015; Bilal et al., 2022; McLennan et al., 1993). The major oxide composition of the Kerman Formation sandstones illustrats arc setting (Figure 11a–b) (Verma & Armstrong-Altrin, 2013); except one sandstone sample contains a composition following the collision setting (Figure 11b). Most samples of the Kerman Formation are low-silica sandstone (Figure 11b).

Most sandstone samples of the Kerman Formation

Table 3. Major elements and calculated indices (CIA and ICV) of the Kerman Formation sandstone samples. Upper continental crust (UCC) values from (Rudnick & Gao, 2003) are used for comparison

Sample No.	SiO_2 wt.%	TiO_2 wt.%	Al_2O_3 wt.%	Fe_2O_{3T} wt.%	MnO wt.%	MgO wt.%	CaO wt.%	Na_2O wt.%	K_2O wt.%	P_2O_5 wt.%	SUM wt.%	LOI wt.%	CIA	ICV
10k	43.09	0.30	8.82	3.50	0.25	4.22	20.48	1.21	1.61	0.06	99.84	16.30	17.71	3.57
17k	61.60	0.40	13.46	4.11	0.11	5.15	4.58	5.21	1.55	0.09	99.80	3.54	42.01	1.56
2	61.51	0.49	13.75	5.57	0.10	5.97	4.00	4.58	1.46	0.08	99.80	2.29	45.62	1.61
15	65.93	0.33	12.65	3.76	0.08	3.60	3.79	4.91	1.88	0.07	99.82	2.78	42.66	1.45
18	54.47	0.57	13.27	6.81	0.13	6.29	6.68	5.54	1.30	0.08	99.78	4.64	36.92	2.05
22	51.99	0.52	11.96	7.15	0.13	7.68	8.94	3.88	1.18	0.10	99.82	6.29	33.33	2.46
25	55.10	0.54	12.09	6.57	0.12	8.38	6.91	4.16	1.08	0.10	99.81	4.76	37.01	2.29
36	52.90	0.56	9.90	8.38	0.18	8.77	9.22	2.02	0.76	0.07	99.74	6.98	32.13	3.01
38	46.92	0.31	8.84	6.08	0.16	6.83	15.82	2.75	0.96	0.08	99.78	11.03	20.47	3.72
UCC	66.62	0.64	15.4	5.04	0.1	2.48	3.59	3.27	2.8	0.15				

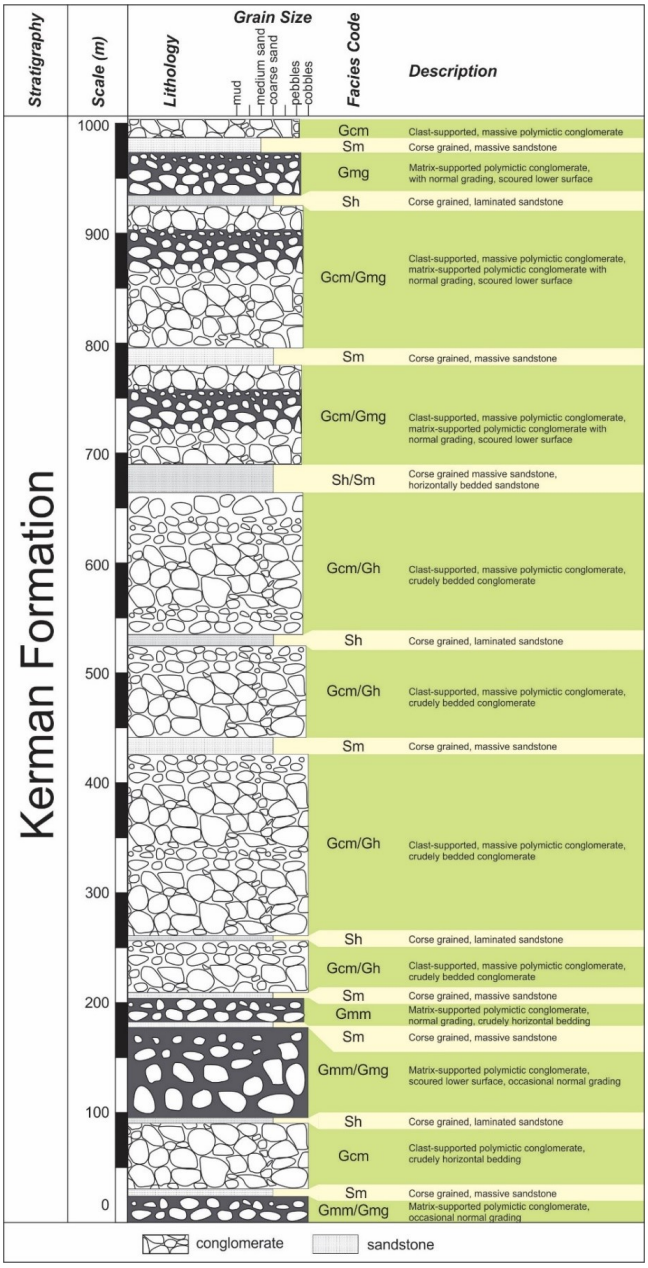

Figure 9. Sedimentary log of the studied section from the Kerman Formation

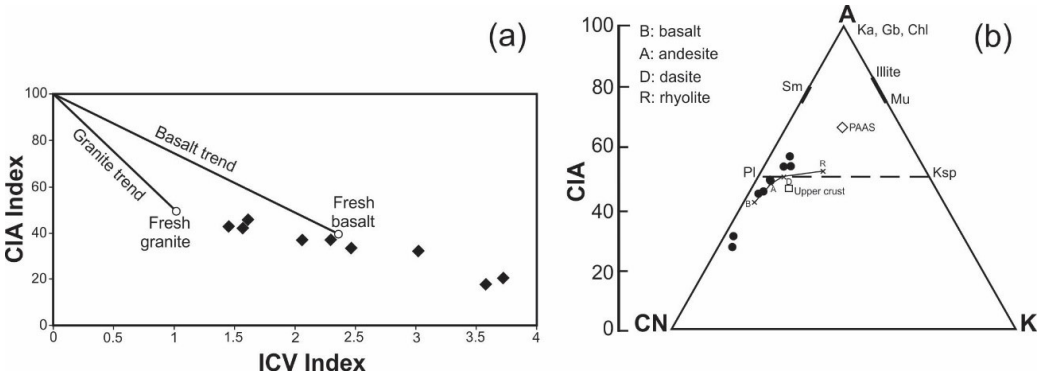

Figure 10. (a) Plot of CIA vs. ICV of the siliciclastic sedimentary rocks of Kerman Formation (Potter et al., 2005). (b) A−CN−K diagram (Nesbitt & Young, 1982) for the Kerman Formation siliciclastic sedimentary rocks. Indices and mineral compositions after Nesbitt and Young (1982): A = Al_2O_3; CN = CaO + Na_2O; and K = K_2O (molar proportions). Sm = smectite; Pl = plagioclase; Ksp = K-feldspar; Ka = kaolinite; Chl = chlorite; Gb = gibbsite; Mu = muscovite. PAAS = Post Archean Australian Shale. Crossed linked by the solid line are average volcanic rock compositions from (Roser et al., 2002). Filled diamonds and circles are sandstone samples from the Kerman Formation

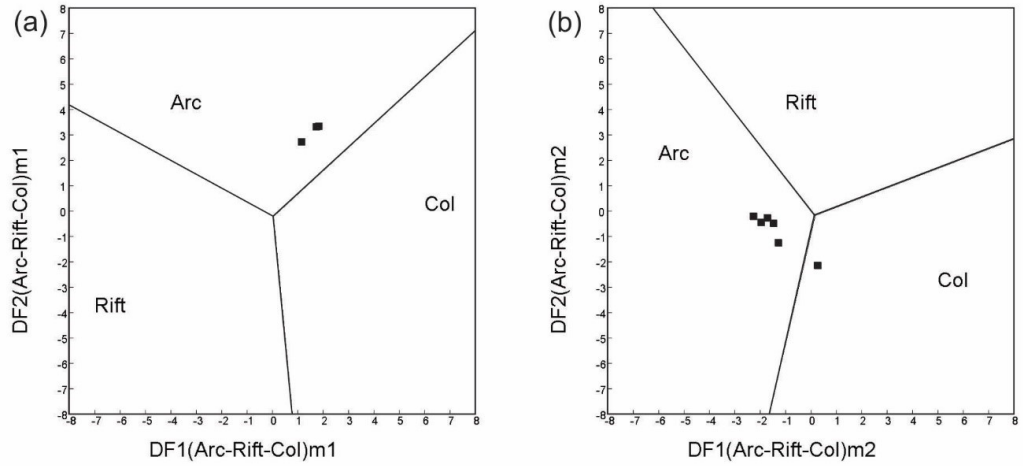

Figure 11. Multidimensional diagram (a) for high silica and (b) low silica sandstone samples of the Kerman Formation after Verma and Armstrong-Altrin (2013)

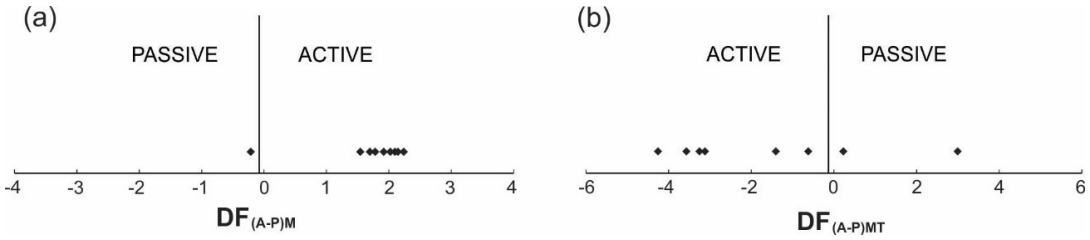

Figure 12. Multidimensional discriminant function diagrams based on (a) major element (M) and (b) combined major and trace element (MT) for the discriminant of active and passive settings after (Verma & Armstrong-Altrin, 2016)

10.57647/j.ijes.2025.16975

reveal a composition under the active margin tectonic setting in a major element-based diagram (Figure 12a). Only one sample contains a conformable composition with the passive margin setting, yet it is located next to the active-passive margin boundary (Figure 12a). The major and trace element-based diagram shows the active margin as the predominant tectonic setting for the Kerman Formation samples except for two sandstone samples showing passive margin (Figure 12b).

Petrographic and geochemical investigations of the Kerman Formation revealed the first-cycled siliciclastic sediments including fresh basalt and andesite in the absence of recycling and alteration, derived from proximal active volcanoes in an arid and cool climate condition. Volcanic detritus of the Kerman Formation can originate from volcanic activities related to the active tectonic setting of Sabzevar oceanic closure and the subduction beneath Eurasia during the Paleocene time.

6. Conclusions

This study discussed the depositional environment and provenance of the Paleocene coarse-grained siliciclastic succession of the Kerman Formation in NE Central Iran examining sedimentological, petrographic, and geochemical investigations. The Kerman Formation contains continental sediments chiefly polymictic conglomerate and coarse-grained sandstone. The six lithofacies were recognized in the Kerman Formation including matrix-supported massive conglomerate, matrix-supported conglomerate, clast-supported massive conglomerate, clast-supported crudely bedded conglomerate, horizontal bedded coarse to fine-grained sandstone, and massive coarse to fine-grained sandstone. Two facies associations demonstrate alluvial fan and proximal braided river systems as the depositional environment. Three petrofacies of petromict conglomerate, volcanic arenite, and feldspathic litharenite were determined. Major and trace element geochemistry on sandstone samples showed the near absence of intense alteration and recycled materials and evidenced cool and arid climate conditions. Petrographic and geochemical investigations of the Kerman Formation revealed the first-cycled siliciclastic sediments including fresh basalt and andesite. Volcanic arc source areas in an active margin tectonic setting were also inferred based on the geochemical data. Volcanic detritus of the Kerman Formation may originate from volcanic activities associated with the active tectonic setting of the Sabzevar oceanic closure and subduction beneath Eurasia during the Paleocene period.

Acknowledgments

The present paper is a part of the third author's master thesis, partially supported by the University of Hormozgan. The anonymous journal referees are gratefully acknowledged for their revisions.

Authors contributions
All the authors have participated sufficiently in the intellectual content, conception and design of this work or the analysis and interpretation of the data (when applicable), as well as the writing of the manuscript.

Availability of data and materials
The data that support the findings of this study are available from the corresponding author, upon reasonable request.

Conflict of interests
The author states that there is no conflict of interest.

References

Abdel-Fattah, Z. A., & Sehsah, H. (2023). The upper neoproterozoic lacustrine-fan delta depositional systems associated with braided alluvial fans in the nubian shiels, egypt. *Sedimentary Geology*, *452*, 106426. https://doi.org/10.1016/j.sedgeo.2023.106426

Aghanabati, A. (2004). *Geology of iran* (3rd) [Farsi]. Ministry of Industry; Mine, Geological Survey of Iran.

Akarish, A. M., & El-Gohary, A. M. (2008). Petrography and geochemistry of lower paleozoic sandstones, east sinai, egypt: Implications for provenance and tectonic setting. *Journal of African Earth Sciences*, *52*, 43–54. https://doi.org/10.1016/j.jafrearsci.2008.04.002

Angiolini, L., Gaetani, M., Muttoni, G., Stephenson, M. H., & Zanchi, A. (2007). Tethyan oceanic currents and climate gradients 300 m.y. ago. *Geology*, *35*, 1071–1074. https://doi.org/10.1130/G24031A.1

Armstrong-Altrin, J. S., Machain-Castillo, M. L., Rosales-Hoz, L., Carranza-Edwards, A., Sanchez-Cabeza, J. A., & Ruíz-Fernández, A. C. (2015). Provenance and depositional history of continental slope sediments in the southwestern gulf of mexico unraveled by geochemical analysis. *Continental Shelf Research*, *95*, 15–26. https://doi.org/10.1016/j.csr.2015.01.003

Berberian, M., & King, G. C. P. (1981). Towards a paleogeography and tectonic evolution of iran. *Canadian Journal of Earth Sciences*, *18*(2), 210–265. https://doi.org/10.1139/e81-019

Bhatia, M. R. (1983). Plate tectonics and geochemical composition of sandstones. *Journal of Geology*, *91*, 611–627. https://doi.org/10.1086/628815

Bhatia, M. R., & Crook, K. A. (1986). Trace element characteristics of graywackes and tectonic setting discrimination of sedimentary basins. *Contributions to mineralogy and petrology*, *92*(2), 181–193.

Bilal, A., Mughal, M. S., Janjuhah, H. T., Ali, J., Niaz, A., Kontakiotis, G., Antonarakou, A., Usman, M., Hussain, S. A., & Yang, R. (2022). Petrography and provenance of the sub-himalayan

kuldana formation: Implications for tectonic setting and palaeoclimatic conditions. *Minerals*, *12*, 794. https://doi.org/10.3390/min12070794

Bilal, A., Yang, R., Lenhardt, N., Han, Z., & Luan, X. (2023). The paleocene hangu formation: A key to unlocking the mysteries of paleo-tethys tectonism. *Marine and Petroleum Geology*, *157*, 106508. https://doi.org/10.1016/j.marpetgeo.2023.106508

Boggs, S. J. (2009). *Petrology of sedimentary rocks*. Cambridge University Press. https://doi.org/10.1017/CBO9780511626487

Bröcker, M., Omrani, H., Berndt, J., & Moslempour, M. E. (2021). Unravelling metamorphic ages of suture zone rocks from the sabzevar and makran areas (iran): Robust age constraints for the larger arabia–eurasian collision zone. *Journal of Metamorphic Geology*, *39*, 1099–1129. https://doi.org/10.1111/jmg.12603

Cox, R., & Lowe, D. R. (1995). A conceptual review of regional-scale controls on the composition of clastic sediment and the co-evolution of continental blocks and their sediment cover. *Journal of Sedimentary Research*, *65*, 1–12. https://doi.org/10.1306/D4268009-2B26-11D7-8648000102C1865D

Critelli, S., & Ingersoll, R. V. (1995). Interpretation of neovolcanic versus palaeovolcanic sand grains: An example from miocene deep-marine sandstone of the topanga group (southern california). *Sedimentology*, *42*, 783–804. https://doi.org/10.1111/j.1365-3091.1995.tb00409.x

Critelli, S., Marsaglia, K. M., & Busby, C. J. (2002). Tectonic history of a jurassic backarc basin sequence (the gran cañon formation) based on compositional modes of tuffaceous deposits. *Geological Society of America, Bulletin*, *114*, 515–527. https://doi.org/10.1130/0016-7606(2002)114<0515:THOAJB>2.0.CO;2

Cui, X., Shi, L., Tang, X., Wang, Z., Wang, J., Cheng, L., Li, L., Wang, B., Han, X., & Zhang, K. (2024). Provenance and tectonic settings of the lower permian siliciclastic rocks in central inner mongolia: Implications for the evolution of the paleo-asian ocean. *Marine and Petroleum Geology*, *161*, 106641. https://doi.org/10.1016/j.marpetgeo.2023.106641

Dickinson, W. R., Beard, L. S., Brakenridge, G. R., Erjavec, J. L., Ferguson, R. C., Inman, K. F., Knepp, R. A., Lindberg, F. A., & Ryberg, P. T. (1983). Provenance of north american phanerozoic sandstones in relation to tectonic setting. *The Geological Society of America, Bulletin*, *94*, 222–235. https://doi.org/10.1130/0016-7606(1983)94<222:PONAPS>2.0.CO;2

Fedo, C. M., Nesbitt, H. W., & Young, G. M. (1995). Unraveling the effects of potassium metasomatism in sedimentary rocks and paleosols, with implications for paleoweathering conditions and provenance. *Geology*, *23*, 921–924. https://doi.org/10.1130/0091-7613(1995)023<0921:UTEOPM>2.3.CO;2

Folk, R. L. (1980). *Petrology of sedimentary rocks*. Hemphill Publishing Co.

Gagnon, J. F., & Waldron, J. W. F. (2011). Sedimentation styles and depositional processes in a middle to late jurassic slope environment, bowser basin, northwestern british columbia, canada. *Marine and Petroleum Geology*, *28*, 698–715. https://doi.org/10.1016/j.marpetgeo.2010.06.004

GhasemShirazi, B., Bakhshandeh, L., & Yazdi, A. (2014). Paleoecology of upper cretaceous sediments in central iran, kerman (bondar-e bido section) based on ostracods. *Marine Science*, *4*(2), 49–57. https://doi.org/10.5923/j.ms.20140402.04

Ghosh, S. (2014). Palaeogeographic significance of ferruginous gravel lithofacies in the ajay-damodar interfluve, west bengal, india. *International Journal of Geology, Earth and Environmental Sciences*, *4*, 81–100.

Ghoshal, S., Allan James, L., Singer, M. B., & Aalto, R. (2010). Channel and floodplain change analysis over a 100-year period: Lower yuba river, california. *Remote Sensing*, *2*, 1797–1825. https://doi.org/10.3390/rs2071797

Hashemi Azizi, S. H., Rezaee, P., & Askari, H. (2024). Reconstruction of depositional environment of the paleocene siliciclastic depositions (kerman formation) in the northeast of central iran (kashmar area) using lithofacies and petrofacies. *Applied Sedimentology (Farsi)*, *23*, 175–188. https://doi.org/10.22084/psj.2024.29062.1429

Hashemi Azizi, S. H., Rezaee, P., Jafarzadeh, M., Meinhold, G., Moussavi Harami, S. R., & Masoodi, M. (2018). Early mesozoic sedimentary-tectonic evolution of the central-east iranian microcontinent: Evidence from a provenance study of the nakhlak group. *Geochemistry*, *78*, 340–355. https://doi.org/10.1016/j.chemer.2018.06.003

Huckriede, R., Kursten, M., & Venzlaff, H. (1962). *Zur geologie des gebietes zwischen kerman und sagand (iran)* (Vol. 51). Geologisches Jahrbuch; Niedersachsen, Hannover, Germany: Landesamt f. Bodenforschung.

Ingersoll, R. V., Bullard, T. F., Ford, R. L., Grimm, J. P., Pickle, J. D., & Sares, S. W. (1984). The effect of grain size on detrital modes: A test of the gazzi-dickinson point-counting method. *Journal of Sedimentary Petrology*, *54*, 103–116. https://doi.org/10.1306/212F83B9-2B24-11D7-8648000102C1865D

Jafari, H. R., & Yazdi, A. (2014). Radioactive anomalies in 1:50000 dehbakri sheet, south of kerman province, iran. *Open Journal of Geology*, *4*(8), 399–405. https://doi.org/10.4236/ojg.2014.48031

Kostic, B., Bech, A., & Aigner, T. (2005). 3-d sedimentary architecture of a quaternary gravel delta (sw-germany): Implication for hydrostratigraphy. *Sedimentary Geology*, *181*, 143–171. https://doi.org/10.1016/j.sedgeo.2005.07.004

Lee, K., & Gihm, Y. S. (2023). Downstream changes in floodplain sedimentation and their effects on channel avulsion in stream-dominated alluvial fans: The cretaceous duwon formation in the southern korean peninsula. *Sedimentary Geology*, *465*, 106473. https://doi.org/10.1016/j.sedgeo.2023.106473

Marsaglia, K. M., Barone, M., Critelli, S., Busby, C., & Fackler-Adams, B. (2016). Petrography of volcaniclastic rocks in intra-arc volcano-bounded to fault-bounded basins of the rosario segment of the lower cretaceous alisitos oceanic arc, baja california, mexico. *Sedimentary Geology*, *336*, 138–146. https://doi.org/10.1016/j.sedgeo.2015.11.008

McCall, G. J. I. L. (1985). *Explanatory text of the tahruie quadrangle map 1:250,000* (Vol. 14). Geological Survey of Iran.

McLennan, S. M., Hemming, S., McDaniel, D. K., & Hanson, G. N. Geochemical approaches to sedimentation, provenance and tectonics (M. J. Johnsson & A. Basu, Eds.). In: In *Processes controlling the composition of clastic sediments (special paper 284)* (M. J. Johnsson & A. Basu, Eds.). Ed. by Johnsson, M. J., & Basu, A. Geological Society of America, 1993, pp. 21–40. https://doi.org/10.1130/SPE284-p21

Miall, A. D. (1977). A review of the braided river depositional environment. *Earth Science Reviews*, *13*, 1–62. https://doi.org/10.1016/0012-8252(77)90055-1

Miall, A. D. Lithofacies types and vertical profile models in braided river deposits (A. D. Miall, Ed.). In: In *Fluvial sedimentology* (A. D. Miall, Ed.). Ed. by Miall, A. D. Canadian Society of Petroleum Geology, Calgary, 1978, pp. 597–604.

Miall, A. D. (1985). Architectural-element analysis: A new method of facies analysis applied to fluvial deposits. *Earth Science Reviews*, *22*, 261–308. https://doi.org/10.1016/0012-8252(85)90001-0

Miall, A. D. (2000). *Principles of sedimentary basin analysis*. Springer. https://doi.org/10.1007/978-3-662-03999-1

Miall, A. D. (2006). *The geology of fluvial deposits, sedimentary facies, basin analysis, and petroleum geology (4th corrected printing)*. Springer. https://doi.org/10.1007/3-540-59186-9

Nesbitt, H. W., & Young, G. M. (1982). Early proterozoic climates and plate motions inferred from major element chemistry of lutites. *Nature*, *299*, 715–717. https://doi.org/10.1038/299715a0

Nesbitt, H. W., Young, G. M., McLennan, S. M., & Keays, R. R. (1996). Effects of chemical weathering and sorting on the petrogenesis of siliciclastic sediments, with implications for provenance studies. *Journal of Geology*, *104*, 525–542. https://doi.org/10.1086/629850

Nichols, G. (2009). *Sedimentology and stratigraphy*. Wiley; Blackwell.

Omrani, H., Moazzen, M., Oberhänsli, R., Altenberger, U., & Lange, M. (2013). The sabzevar blueschists of the north-central iranian microcontinent as remnants of the neotethys-related oceanic crust subduction. *International Journal of Earth Sciences*, *102*, 1491–1512. https://doi.org/10.1007/s00531-013-0881-9

Oplustil, S., Martinek, K., & Tasaryova, Z. (2005). Facies and architectural analysis of fluvial deposits of the nyrany member and the tynec. *Bulletin of Geosciences*, *80*(1), 45–66.

Pettijohn, F. J., Potter, P. E., & Siever, R. (1987). *Sand and sandstone*. Springer-Verlag. https://doi.org/10.1007/978-1-4612-1066-5

Potter, E. P., Maynard, J. B., & Depetris, P. J. (2005). *Mud and mudstone: Introduction and overview*. Springer-Verlag. https://doi.org/10.1007/b138571

Roser, B. P., Coombs, D. S., Korsch, R. J., & Campbell, J. D. (2002). Whole-rock geochemical variation and evolution of the arc-derived murihiku terrane, new zealand. *Geological Magazine*, *139*, 665–685. https://doi.org/10.1017/S0016756802006945

Roser, B. P., & Korsch, R. J. (1988). Provenance signatures of sandstone-mudstone suites determined using discriminant function analysis of major-element data. *Chemical geology*, *67*(1-2), 119–139.

Rossetti, F., Nasrabady, M., Vignaroli, G., Theye, T., Gerdes, A., Razavi, M. H., & Vaziri, H. M. (2010). Early cretaceous migmatitic mafic granulites from the sabzevar range (ne iran): Implications for the closure of the mesozoic peri-tethyan oceans in central iran. *Terra Nova*, *22*(1), 26–34. https://doi.org/10.1111/j.1365-3121.2009.00912.x

Rudnick, R. L., & Gao, S. Composition of the continental crust (H. D. Holland & K. K. Turekian, Eds.). In: In *Treatise on geochemistry* (H. D. Holland & K. K. Turekian, Eds.). Ed. by Holland, H. D., & Turekian, K. K. Elsevier-Pergamon, 2003, pp. 1–64. https://doi.org/10.1016/B0-08-043751-6/03016-4

Sallam, E. S., Garzanti, E., Li, X., & Ruban, D. A. (2022). Provenance of mesozoic sandstones from the northwestern gulf of suez, egypt: New evidence from petrography and whole-rock geochemistry. *Arabian Journal of Geosciences*, *15*, 1004. https://doi.org/10.1007/s12517-022-10256-6

Sallam, E. S., & Ruban, D. A. (2021). Provenance, tectonic setting and source area palaeoweathering of the lower cretaceous nubian sandstones at gebel duwi, eastern desert, egypt: Inferences from mineralogy and whole-rock geochemistry. *Arabian Journal of Geosciences*, *14*, 2400. https://doi.org/10.1007/s12517-021-08743-3

Sallam, E. S., & Wanas, H. A. (2019). Petrography and geochemistry of the jurassic siliciclastic rocks in the khashm el-galala area (nw gulf of suez, egypt): Implication for provenance, tectonic setting and source area paleoweathering. *Journal of African Earth Sciences*, *160*, 103607. https://doi.org/10.1016/j.jafrearsci.2019.103607

Sangeeta, A., Kingson, O., Yadav, B. S., Pandey, N., & Meitei, N. R. (2023). Geochemistry of the siliciclastic sediments in the barak basin, indo-burma range, india: Insights into provenance, paleoclimate, and depositional history. *Journal of Asian Earth Sciences X*, *10*, 100161. https://doi.org/10.1016/j.jaesx.2023.100161

Seyed-Emami, K. (1972). Upper cretaceous in iran. *Journal of the College of Engineering (Farsi)*, *22*, 7–34.

Shafaii Moghadam, H., Corfu, F., Chiaradia, M., Stern, R. J., & Ghorbani, G. (2014). Sabzevar ophiolite, ne iran: Progress from embryonic oceanic lithosphere into magmatic arc constrained by new isotopic and geochemical data. *Lithos*, *210-211*, 224–241. https://doi.org/10.1016/j.lithos.2014.10.004

Shafaii Moghadam, H., Zaki Khedr, M., Arai, S., Stern, R. J., Ghorbani, G., Tamura, A., & Ottley, C. (2015). Arc-related harzburgite–dunite–chromitite complexes in the mantle section of the sabzevar ophiolite, iran: A model for the formation of podiform chromitites. *Gondwana Research*, *27*, 575–593. https://doi.org/10.1016/j.gr.2013.09.007

Shahrabi, M. (2010). Bardeskan 1:100000 quadrangle map, no 7560.

Smith, J. J., & Platt, B. F. (2023). Reconstructing late miocene depositional environments in the central high plains, usa: Lithofacies and architectural elements of the ogallala formation. *Sedimentary Geology*, *443*, 106303. https://doi.org/10.1016/j.sedgeo.2022.106303

Sridhar, A., Chamyal, L. S., Bhattacharjee, F., & Singhvi, A. K. (2013). Early holocene fluvial activity from the sedimentology and palaeohydrology of gravel terrace in the semi-arid mahi river basin, india. *Journal of Asian Earth Sciences*, *66*, 240–248. https://doi.org/10.1016/j.jseaes.2013.01.017

Verma, S. P., & Armstrong-Altrin, J. S. (2013). New multi-dimensional diagrams for tectonic discrimination of siliciclastic sediments and their application to precambrian basins. *Chemical Geology*, *355*, 117–180. https://doi.org/10.1016/j.chemgeo.2013.07.014

Verma, S. P., & Armstrong-Altrin, J. S. (2016). Geochemical discrimination of siliciclastic sediments from active and passive margin settings. *Sedimentary Geology*, *332*, 1–12. https://doi.org/10.1016/j.sedgeo.2015.11.011

Zhang, Y., Colombera, L., Mountney, N. P., Gao, C., Ji, Y., Wu, H., Du, W., Liu, D., Bai, D., & Song, W. (2021). Sedimentation of open-framework gravels in alluvial-fan settings: Quaternary polar fan, northwest china. *Marine and Petroleum Geology*, *134*, 105376. https://doi.org/10.1016/j.marpetgeo.2021.105376

Zhang, Y., Dai, X., Wang, M., & Li, X. (2020). The concept, characteristics and significance of fluvial fans. *Petroleum Exploration and Development*, *47*(5), 1014–1026. https://doi.org/10.1016/S1876-3804(20)60113-6